Mechanism and Design Principles for Controlling Stereoselectivity in the Copolymerization of CO_2/Cyclohexene Oxide by Indium(III) Phosphasalen Catalysts

Yernaidu Reddi* and Christopher J. Cramer

Department of Chemistry, Chemical Theory Center, and Supercomputing Institute, University of Minnesota, 207 Pleasant St. SE, Minneapolis, Minnesota 55455, United States

ABSTRACT: Copolymerization of CO_2 with cyclohexene oxide (CHO) creates a sustainable polymer that has been a target for homogeneous catalysis. In particular, indium(III) phosphasalen catalysts generate high proportions of carbonate linkages in isotactic product poly(cyclohexene carbonate) (*i*PCHC). We use theory here to characterize the initiation and propagation steps for these indium(III) catalysts which involve mononuclear mechanisms for CO_2 insertion and CHO ring-opening that are distinct from copolymerization mechanisms previously reported for other metal-based catalysts. We find that phosphasalen ligand interactions with CHO and the carbonate-terminated growing chain lead to stereoselection for high levels of isotacticity and suggest further modifications to the ligand that might tune this.

Keywords: *density functional theory, ring-opening copolymerization, phosphasalen ligands, noncovalent interactions, ligand modification, isoselectivity, reaction mechanism*

Introduction

CO_2 is a renewable, inexpensive, abundant feed stock and C1 building block. The capture and use of CO_2 in value-added products is one of the key goals of sustainable and green chemistry and an emerging and challenging task for the reduction of global warming.[1] In 1969, Inoue *et al*. synthesized polycarbonates (PCs) from the ring-opening copolymerization (ROCOP) of epoxides and CO_2, this being one of the most efficient ways to utilize CO_2.[2] PCs are value-added products that can serve as thermoplastics in a wide

range of applications including ceramic binders, adhesives, coatings, elastomers, and packaging materials.[3] To date, many metal catalysts have been documented for the synthesis of atactic PCs, in addition to thermodynamically stable cyclic carbonates from a competing 1:1 reaction of epoxides and CO_2.[4] Atactic PCs have more limited applications than stereoregular polymer owing to the poorer mechanical and thermal properties of the former.[5,6] As such, the search for catalysts able to achieve high levels of ROCOP reactivity and isotacticity has been a priority.

Mono- and binuclear homogeneous metal-based catalysts, supported by salen, β-diiminate, and porphyrin ligands, amongst others, have been described for the synthesis of poly(cyclohexene carbonate) (PCHC) from ROCOP of cyclohexene oxide (CHO) and CO_2. Research has focused on achieving high fractions of carbonate linkages (vs polyether formation), turn-over frequencies (TOF), isotacticity, and minimal dispersity.[7] Recent metal-based catalysts incorporating phosphasalen ligands have shown promising reactivity, selectivity, and dispersity control for a variety of polymerization reactions.[8] Of special note, Williams and co-workers reported the capture of CO_2 in a copolymerization process, using CHO to generate isotactic PCHC (*i*PCHC), catalyzed by indium(III) phosphasalen catalysts (Scheme 1).[9] They observed that their phosphasalen catalysts performed better than corresponding salen catalysts in terms of both reactivity and selectivity. Indeed, they reported the preparation of *i*PCHC having >99% carbonate linkages and 76% isotacticity (P_m) for the ROCOP of CHO/CO_2 using the indium(III) phosphasalen catalyst **C1** at 60°C and 1 bar CO_2 pressure (Scheme 1).[9] They successfully isolated and characterized key intermediates to help illuminate the mechanism, and our goal, here, is to expand understanding of individual microscopic steps – and factors controlling stereoselectivity – through computational modeling. Theoretical contributions to elucidating mechanistic and stereochemical details for other metal-catalyzed ROCOP reactions are extant,[10] although this is the first to examine indium(III) phosphasalen catalysts. In addition to exploring the specific experimental system, we employ theory to evaluate the utility of possible catalyst modifications.

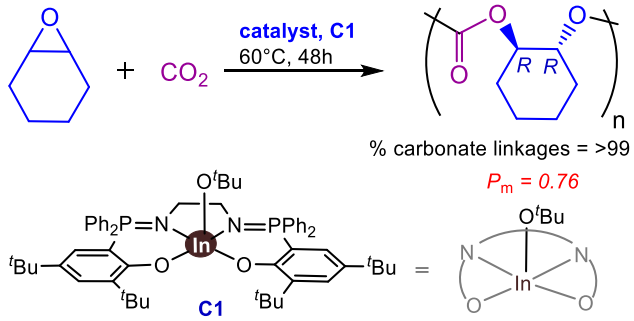

Scheme 1. Ring-opening copolymerization of cyclohexene oxide and CO_2 using an indium(III) phosphasalen catalyst.

Computational Details

All stationary-point structures were optimized at the M06-L[11] level of density functional theory including Grimme's D3 dispersion[12] and using the mixed basis set SDD[13] for In and Br (with associated core pseudopotentials) and 6-31+G(d) for all other atoms. Optimizations were carried out including solvent effects using the SMD solvation model[14] for dichloromethane (DCM; $\varepsilon = 8.93$). Computations used the *Gaussian16* suite of electronic structure programs.[15] To verify the nature of stationary points, as well as to compute partition functions for use in free energy calculations, analytical vibrational frequency calculations were undertaken. All TS structures were confirmed to have exactly one imaginary frequency. Intrinsic Reaction Coordinate (IRC) calculations for TS structures were used to connect them to respective reactants and products. For improved energy-estimates, single-point calculations were then carried out using the SMD solvation model at the M06,[11] ωB97X-D,[16] PBE0-D3,[17] and MN15[18] levels of theory using a mixed basis set of def2-TZVP with pseudopotential for In and Br and 6-31++G(d,p) for all other atoms. Gibbs free energies for all stationary points were obtained by adding the zero-point vibrational energy (ZPVE) and thermal energy corrections from standard statistical mechanics approximations at 333.15 K and 1 atm pressure, except that vibrational modes below 100 cm^{-1} were replaced with a value of exactly 100 cm^{-1} in vibrational partition function calculations. Computed 333.15 K Gibbs free energies at the $SMD_{(DCM)}$/ωB97X-D/6-31++G(d,p),def2-TZVP|SDD(In)//$SMD_{(DCM)}$/M06-L-D3/6-31+G(d),SDD(In)

level are used for discussion in the main text, with results from other levels of theory described in the Supporting Information.

As employed experimentally, catalyst **C1** has equal populations of Δ and Λ enantiomers in solution, but stereochemical control of polymer tacticity can derive from the influence that catalyst chirality exerts on locally diastereomeric transition-state structures for ring opening (and further control can derive from the chirality of the locally growing chain). To facilitate discussion of our computational results, we will work exclusively with Δ catalyst chirality, noting that all energetics would be exactly equivalent for mirror-image structures associated with Λ catalyst; we will focus on the degree to which local catalyst and growing-chain stereochemistry affects the energetics of alternative initiation and propagation pathways.

Results and Discussion

We examine first the initiation of CO_2/CHO ROCOP with a **C1** catalyst having O^{t}Bu as the initiator. Two alternative pathways may be imagined, deriving from initial coordination of either CHO or CO_2 to the indium center of the **C1** catalyst and then subsequent steps. However, the former process is energetically uncompetitive with the latter, and we relegate its description to the Supporting Information (Scheme S1 and Figure S1). With respect to initiation beginning from CO_2 insertion, Scheme 2 provides an overview of the process.

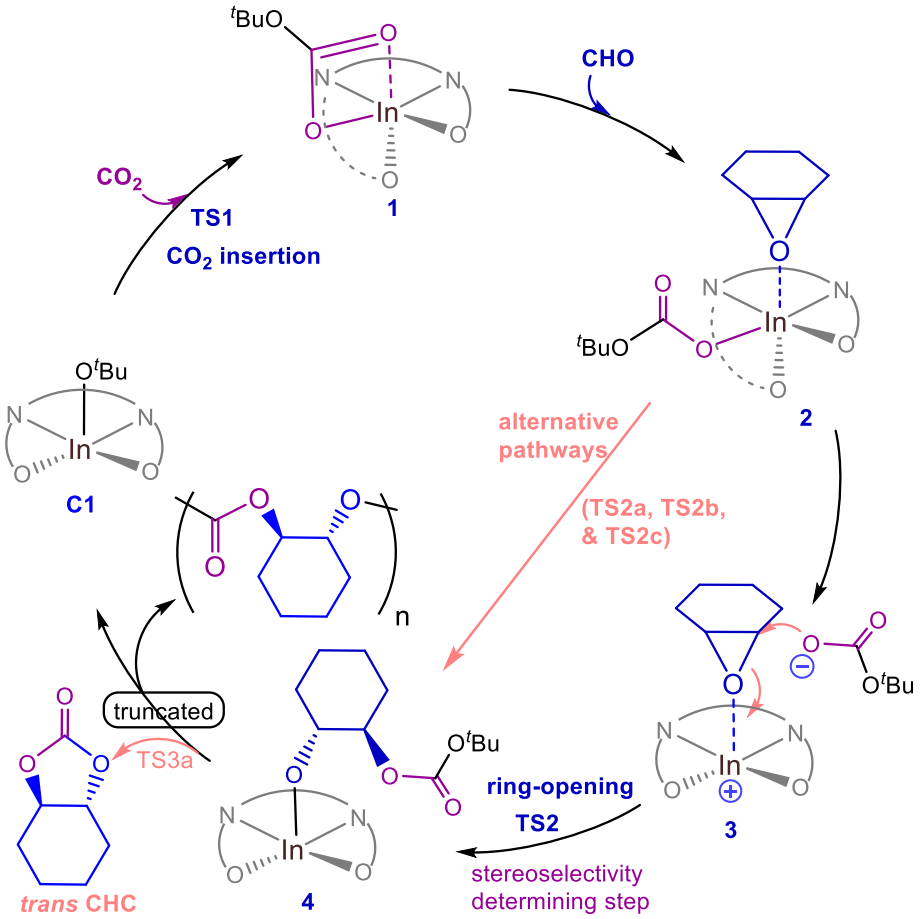

Scheme 2. Key mechanistic steps involved in the initiation cycle for ring-opening copolymerization of CO_2/CHO catalyzed by **C1**.

Specifically, CO_2 associates initially with **C1** to form a Van der Waals complex, from which CO_2 insertion occurs through a four-membered ring transition-state (TS) structure **TS1** to generate hexa-coordinate indium(III) carbonate intermediate **1**. Two conformationally distinct TS structures were characterized for CO_2 insertion (Figure 1), differing by orientation of the inserting CO_2. Conformation Δ_{c1} (**TS1**) is the lower energy TS structure with a free energy of activation of 11.8 kcal/mol. The lowest-energy conformation of **1** is 4.5 kcal/mol below educts **C1** and CO_2 (Supporting Information, Figure S2) and involves octahedral coordination at the metal including a chelating (κ^2) carbonate and *cis*-β phosphasalen, consistent with experimental analysis.[9] Next, CHO displaces one weakly coordinated

carbonate oxygen at indium to generate intermediate **2**. Of several possible conformations for **2**, the lowest in energy is 1.7 kcal/mol below educts **C1**, CO_2 and CHO (Supporting Information, Figure S3).

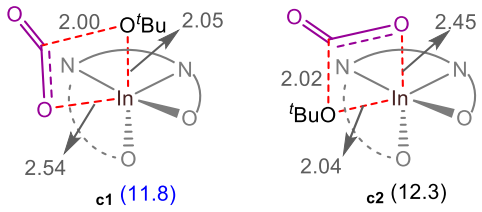

Figure 1. Possible initiation transition-state structures for CO_2 insertion together with free energies of activation relative to **C1** and CO_2 (kcal/mol; 333.15K) and selected bond distances (Å).

Intermediate **2** next undergoes ring-opening of CHO to give intermediate **4**, and we characterized four different pathways for this process (**TS2**, **TS2a**, **TS2b**, and **TS2c**; Figures 2, S4–S6; Supporting Information), two intramolecular and two intermolecular. The intramolecular paths involve substitution of either of the two oxygens of the indium-coordinated carboxylate at CHO with concomitant epoxide ring opening to a coordinated alkoxide product. Unsurprisingly, the activation free energies associated with these two transition state structures are quite high (**TS2a**, 38.9 kcal/mol; **TS2b**, 37.4 kcal/mol) as a backside attack geometry cannot be achieved for the nucleophilic substitution (leading to product *cis*-**4** as opposed to *trans*-**4**). In contrast, if carboxylate is fully dissociated from indium, an ion-pair intermediate **3** is readily found from which backside attack *can* occur, and the free energy of activation is substantially lower at 27.3 kcal/mol (**TS2**; cf. Table S1 and Figure S6 for complete analysis of conformational alternatives for this step and discussion in the Supporting Information). To assess the potential for free carboxylate to interact with a *different* catalyst to which a separate carboxylate terminus remains coordinated, we characterized relevant nucleophilic ring-opening pathways as well. The reduced Lewis acidity of the catalyst in this instance increases the free energy of activation via **TS2c** to 30.0 kcal/mol. Overall, then, as shown in Figure 3, CHO ring-opening is computed to be rate-determining for initiation, with a 333.15 K standard-state free energy of activation of 30.1 kcal/mol relative to intermediate **1**.

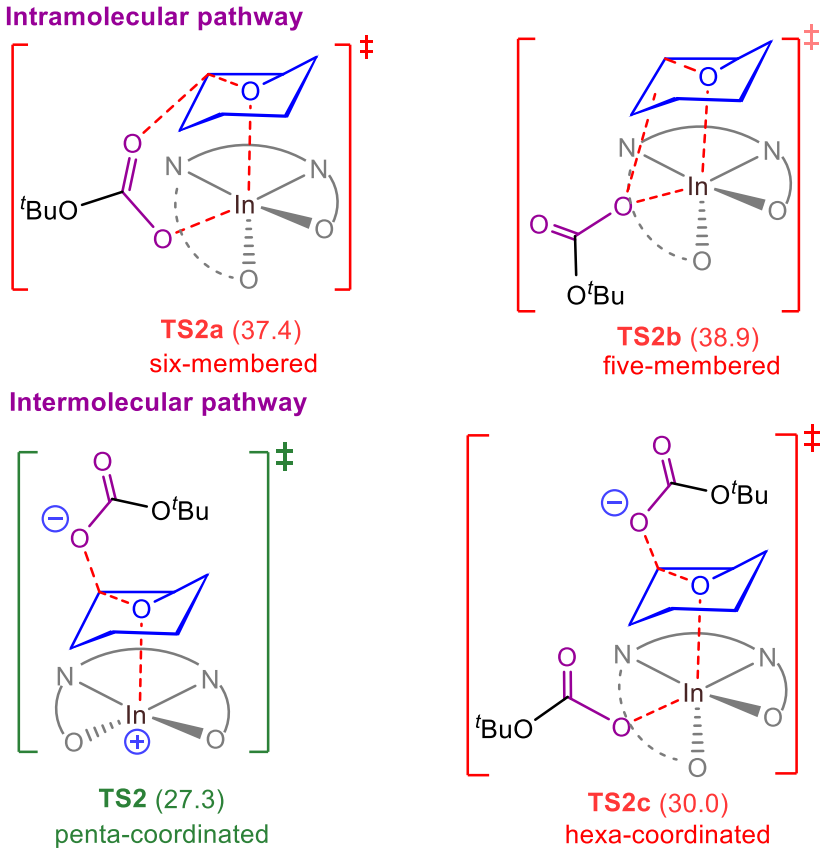

Figure 2. Ring-opening transition-state structures and associated free energies of activation (kcal/mol; 333.15 K) relative to **2** for intra- and intermolecular initiation pathways.

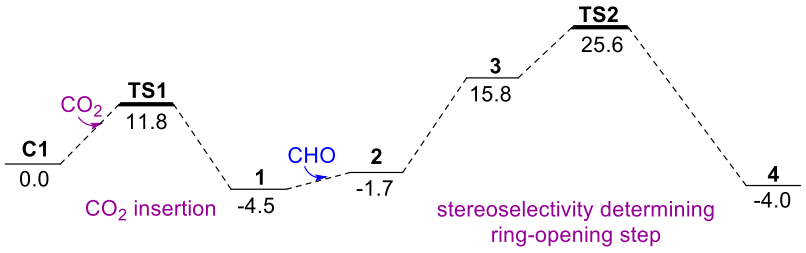

Figure 3. Reaction coordinate with associated free energies (333.15K; kcal/mol) for initiation of ring-opening copolymerization of CO_2/CHO catalyzed by **C1.**

Of particular importance in this process is the degree to which the chirality of the indium catalyst (chosen for computational purposes as Δ) influences the *R,R* vs *S,S* chirality of the diol linkage in product **4**, as site-control of isotacticity will depend on the relative energetics of alternative ring-opening pathways leading to diastereomeric intermediates **4**. In total, 40 conformationally distinct TS structures were identified distinguished by orientation of the carbonate nucleophile, rotation of CHO around the indium metal site, and, of course, site of nucleophilic attack (Figures 4, S6, and Table S1 in the Supporting Information). From this set, the lowest-energy TS structure that leads to *R,R* stereochemistry (**TS2**$_{RR}$) is predicted to be 1.1 kcal/mol lower in free energy than the corresponding lowest-energy TS structure that leads to *S,S* stereochemistry (**TS2**$_{SS}$). Considering the Boltzmann average over both sets of TSs, the difference drops slightly to 0.9 kcal/mol. This value agrees well with that found experimentally, 1.3 kcal/mol.[9]

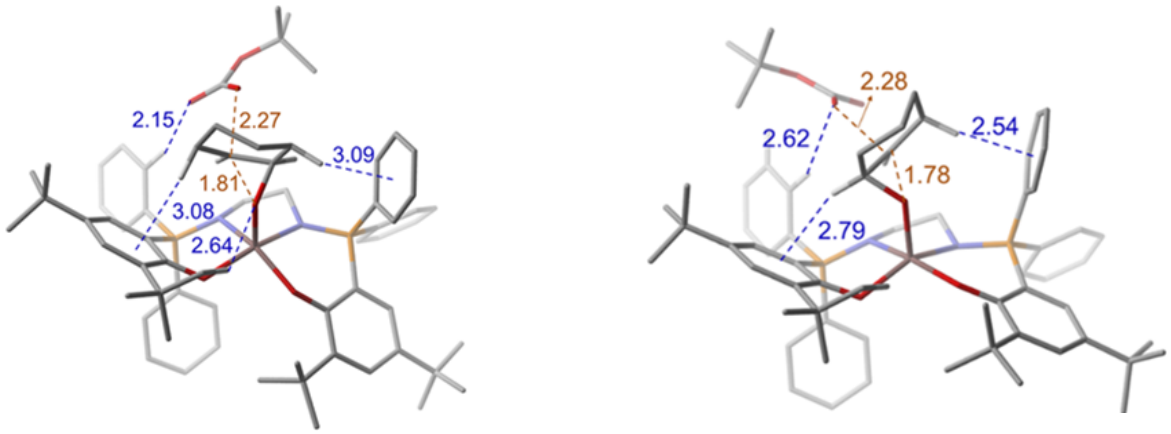

TS2$_{RR}$ (0.0) [0.0] **TS2**$_{SS}$ (1.1) [0.9]

Figure 4. Lowest-energy transition-state structures leading to diastereomeric intermediates **4** with associated relative free energies (333.15 K; kcal/mol) and selected bond distances (Å). Computed Boltzmann weighted free energies are provided in square brackets.

We further assessed **TS2**$_{RR}$ and **TS2**$_{SS}$ to try better to understand the factors affecting selectivity. CM5 partial atomic charge analysis[19] gives In partial charges of +0.631 for **TS2**$_{RR}$ and +0.645 for **TS2**$_{SS}$, suggesting little difference in early vs late character for ring-opening in the competing TS structures.

Interestingly, the *electronic* energy difference for these two structures is computed to be very small (0.1 kcal/mol; Supporting Information, Table S2), i.e., the computed free-energy difference derives essentially entirely from thermal effects associated with the alternative vibrational partition functions. In effect, the "looser" **TS2*RR*** is characterized by a number of normal modes computed at slightly lower-frequency than those in corresponding **TS2*SS***, the summed additional entropy from which lower the net free energy by 1 kcal/mol. While somewhat dissatisfying, in the sense that one cannot point to a single, clearly controlling factor for stereoselection in ring-opening, this result is important to the extent it suggests that modifications of the catalyst ligand structure that might further constrain the *S,S* TS structure(s) relative to the *R,R* could lead to enhanced selectivity. It is not a priori obvious what such modifications might be, but computational exploration permits us to test various alternatives, as discussed further below. Further, intermediate **4** can either form *trans* cyclohexene carbonate (CHC) or continue propagation (Schemes 2 and 3). The free energy of activation for the formation of *trans* CHC from **4** *via* **TS3a** is 37.0 kcal/mol (Supporting Information; Figure S7) and the reaction is exergonic by 1.7 kcal/mol.

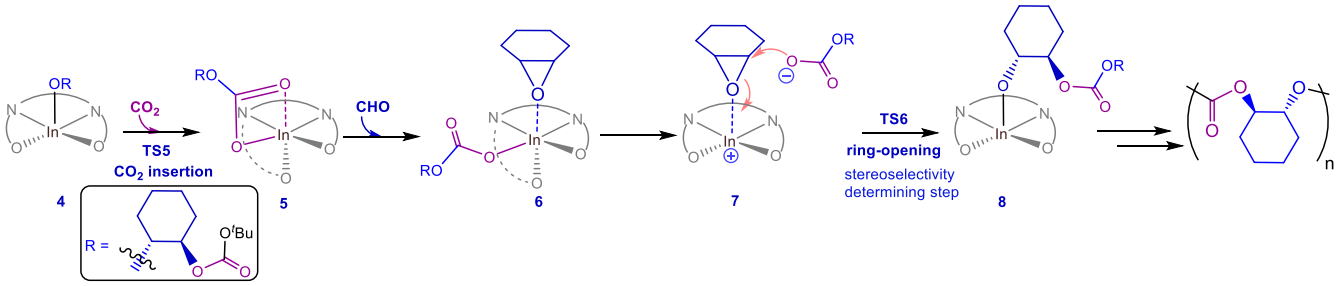

Scheme 3. Key mechanistic steps involved in the propagation cycle for ring-opening copolymerization of CO_2/CHO catalyzed by **C1**.

First, however, as our work thus far focused on initiation, we proceeded to verify that propagation, using an appropriate cyclohexylcarbonate nucleophile as opposed to a *t*-butylcarboxylate, had no significant impact on the relevant reaction coordinate(s). As shown in Scheme 3 and Figure 5, and with further details in Supporting Information (Figures S8 and S9 and Table S3), propagation differs from initiation only modestly from an energetic standpoint. The slightly more crowded nature of **4** relative to **1** causes the standard-state free-energy of activation for the former to be 14.8 kcal/mol compared to 11.8 kcal/mol for the latter, but this is still well below rate-determining CHO ring opening. By contrast, ring-opening itself proceeds with a *lower* standard-state free energy of activation for propagation compared to initiation, 26.6 kcal/mol via **TS4** vs 30.1 via **TS2**. This difference is primarily attributable to the greater facility of charge separation, leading to the ion-pair intermediate **7** vs **3** and subsequent TS structures, when the carbonate itself is larger and better able to distribute charge in the anion. Finally, the net free energy of propagation is predicted to be very slightly endergonic, but this is in part simply an artifact of the standard-state convention, which assumes an equimolar concentration of CHO and catalyst for purposes of computation — experimentally, excess substrate relative to catalyst obviously helps drive polymerization. In addition, however, it is fairly typical for electronic structure calculations to underestimate the full entropy associated with a growing polymer chain (i.e., an intrinsically thermochemical contribution as opposed to an electronic one), and this, too, leads to reduced predicted exergonicity.[20] It is also evident from the energetics noted above that the formation of *trans* CHC from **4** is vastly less likely compared to propagation.

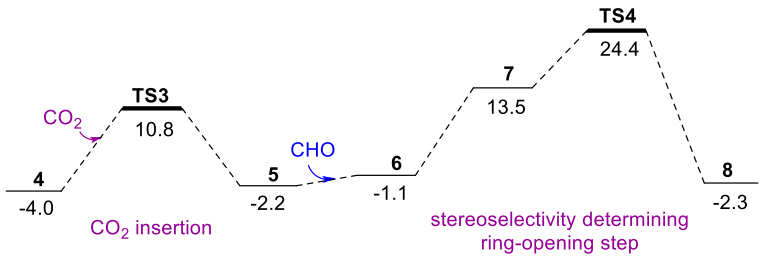

Figure 5. Gibbs free energy (at 333.15K in kcal/mol) profile for propagation cycle for ring-opening copolymerization of CO_2/CHO catalyzed by **C1**.

Returning to the question of site-control of stereoselection, 53 conformationally distinct TS structures were located leading to *R,R* or *S,S* stereochemistry at the *new* diol unit (Figure 6, S9 and Table S3 for complete conformational analysis and discussion in the Supporting Information). The lowest in energy (**TS4**$_{RRRR}$) was found to lead to *RRRR* product, consistent with experimental preference for isotacticity (note that we identify stereocenters in order from furthest position relative to the catalyst to nearest). The free energy of activation associated with the lowest energy ring-opening TS leading to a locally *mismatched* linkage (**TS4**$_{RRSS}$) is computed to be 0.8 kcal/mol higher in energy. The Boltzmann averaged difference is 1.1 kcal/mol. This value is effectively the same as that reported above for initiation.

When stereochemical outcomes are dictates by relatively small energy differences, it is often difficult to identify decisive contributions to those differences, particularly in complex structures. In the case of the TS structures leading to *RRRR* vs *RRSS* product, this is certainly the case, but a careful analysis of various interatomic differences (Figure 6) does suggest that there are more and shorter interactions between C–H hydrogen atoms and electronegative elements (oxygen atoms of the carboxylate nucleophile or nitrogen atoms of the ligand) in the *RRRR* TS structure than in the *RRSS* TS structure.

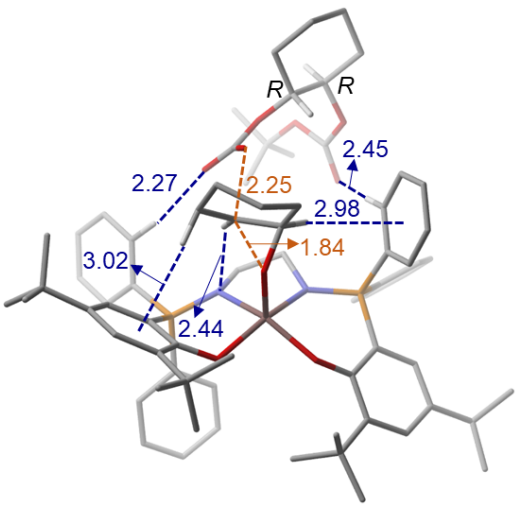

TS4*RRRR* (0.0) [0.0]

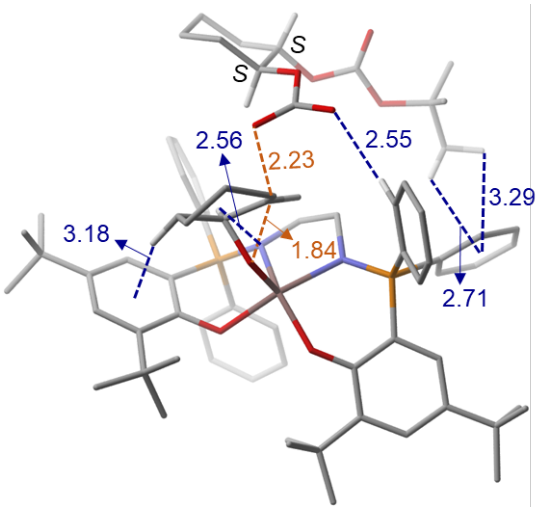

TS4*SSSS* (1.7) [1.8]

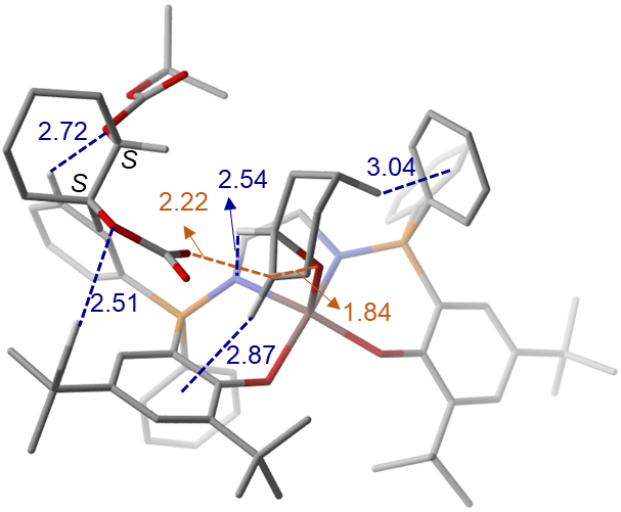

TS4*SSRR* (0.7) [0.6]

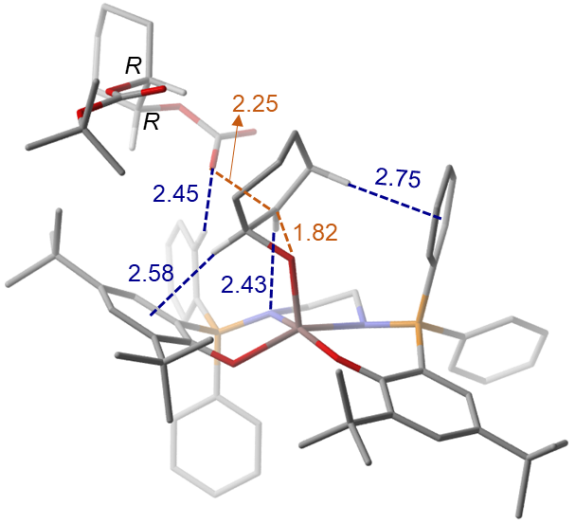

TS4*RRSS* (0.8) [1.1]

Figure 6. Lowest-energy optimized TS structures for ring-opening of CHO in the propagation cycle including selected bond distances (Å). Relative free energies of activation ($\Delta\Delta G^{\ddagger}$; kcal/mol) are in parentheses; Boltzmann weighted free energies of activation are provided in square brackets.

As propagation requires dissociation of the growing polymer chain from the catalyst, followed by attach *by* that chain on coordinated CHO, it is appropriate to ask the question of the degree to

which "escape" of the growing chain from a tight ion pair might permit loss of stereoregularity through attack of an *SS* nucleophile on a catalyst otherwise disposed to favor *RR* ring-opening based on site control. As shown in Figure 6, with an *SS* nucleophile, there is a preference to generate new *RR* stereocenters by essentially precisely the same amount as with an *RR* nucleophile, i.e., ~1.1 kcal/mol. However, the considerably different coordination of CHO to the catalyst in all 4 TS structures suggests that this is more coincidental than owing to any consistent difference in site interactions with either or both substrates.

In addition, there is a difference in activation free energies leading to *SSRR* vs *RRRR* of 0.7 (or 0.6, Boltzmann averaged) kcal/mol. This difference is above and beyond any effective free energy barrier associated with escape of the anionic growing polymer chain from the cationic uncoordinated catalyst. We sought further to understand the stereoselective controlling factors that are responsible for the difference in relative free energy of 1.7 (or 1.8, Boltzmann averaged) kcal/mol between the two lower energy ring-opening TS structures T**S4**$_{RRRR}$ and **TS4**$_{SSSS}$ in the propagation cycle (Figure 6). Various weak non-covalent interactions such as C-H…O, C-H…N, and C-H…π interactions between the phosphasalen ligand and CHO and carbonate linkers are identified in both TS structures, **TS4**$_{RRRR}$ and **TS4**$_{SSSS}$. The difference in strength of these interactions between these TS structures are stereocontrolling factors for the observed isoselectivity. A non-covalent interaction (NCI) plot[21] was used to examine and analyze these weak intramolecular interactions in **TS4**$_{RRRR}$ and **TS4**$_{SSSS}$ (See Figure S10 in the Supporting Information). The computations indicate overall, then, that site control is dominant over chain-end control with respect to influence on the stereochemistry of ring-opening of the CHO monomer.

Effect of Ligand Substituents on Reactivity and Isoselectivity

Having characterized in detail the initiation and propagation cycles of the **C1** catalyst, we next undertook computational predictions of the stereoselectivity of ring-opening for catalysts modified with various substituents at the *ortho* and *para* positions of the phenolate groups as well as varying the aryl groups of the phosphasalen ligand, noting the utility of other DFT studies with respect to the rational design of catalyst/ligand systems having improved reactivity and selectivity.[10a,22] In total, 34 ligands were assayed to discern their propensity for enhanced reactivity and/or stereoselectivity for ROCOP. The free energies of activation and differences in *relative* free energies of ring-opening steps determining stereoselectivity are provided in the Supporting Information (Table S4). Here, we first compare our predictions to results from experimentally reported catalysts and follow with a discussion of predictions for other possible ligands/substituents.

Validations on Experimentally Available Catalysts: Experiments were performed with catalysts where the ^{t}Bu groups of the phenolate rings were replaced with amyl and cumyl substituents at the *ortho* and *para* positions of the **C1** catalyst, these being denoted as **C2** and **C3** catalysts, respectively (Supporting Information; Figure S11 and Table S4). We compare TS structures (e.g., **TS2*RR*** and **TS2*SS***) for the initiation cycle noting the close agreement of initiation and propagation predictions for **C1**. As a technical point, the considerably increased number of conformations of the amyl and cumyl groups compared to *t*-butyl groups rendered these computations more time consuming, but we exhaustively explored the relevant conformational spaces.

We found that *R,R* stereoselection continued to be preferred for Δ catalysts for both **C2** and **C3** (energetic details of conformational TSs are provided in Table S5 and Table S6; Supporting Information). The differences in relevant activation free energies for the **C2** and **C3** catalysts are 1.6 and 2.4 kcal/mol, respectively (1.4 and 2.3 kcal/mol Boltzmann averaged). These values are in

good agreement with reported values of 1.3 and 2.0 kcal/mol, respectively. In addition, the free energies of activation for the ring-opening steps for the **C2** and **C3** catalysts are computed to be 25.9 kcal/mol and 24.9 kcal/mol, respectively, consistent with their reported enhanced activity relative to **C1**.

To understand the origin of enhanced isotacticity with cumyl groups, we analyzed the ring-opening TS structures **TS2*RR*_C3** and **TS2*SS*_C3** (Figure S12 in the Supporting Information) using distortion and interaction energy analysis. We found the distortion energy in **TS2*SS*_C3** is 7.7 kcal/mol greater than in **TS2*RR*_C3**. While this is offset by an interaction energy that is 5.5 kcal/mol more favorable for **TS2*SS*_C3** (Figure S13 in the Supporting Information), the greater influence of the distortion energy favors **TS2*RR*_C3**. Importantly, the difference in phosphasalen ligand distortion energy for **C3** is 4.1 kcal/mol larger than for **C1**, suggesting that the cumyl groups improve structural flexibility to accommodate one stereoisomer relative to the other compared to *t*-butyl groups (Figure S13 in the Supporting Information).

We also examined replacing the ^{t}Bu groups at the phenolate *para* positions with various electron-withdrawing and electron-donating substituents (**C4**-**C12**). None of these catalysts were predicted to be improved over the **C3** catalyst, however, electron donating substituents at the *para* position of the phenolate groups *were* predicted to be more reactive and more stereoselective than electron withdrawing substituents, but dramatic improvements relative to **C3** were not realized.

Table 1. Effects of Selected Phosphasalen Ligand Phenolate Substituents (R_1 and R_2) and Phenyl Groups (Ar) on Free Energies (kcal/mol) of Reactivity ($\Delta G^{\ddagger}$) and Isoselectivity ($\Delta\Delta G$) for Initiation of the CO_2/CHO Copolymerization Reaction

catalyst	**R_1**	**R_2**	**Ar**	**$\Delta G^{\ddagger}$**	**$\Delta\Delta G$**	

C1	^{t}Bu	^{t}Bu	Ph	27.3	1.1	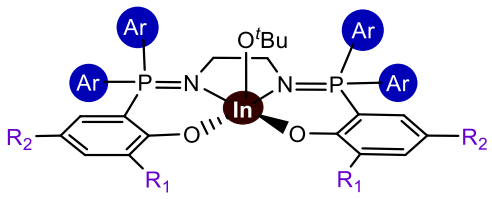
C3	cumyl	cumyl	Ph	24.9	2.4	
C25	^{t}Bu	^{t}Bu	Mesityl	25.4	2.6	
C35	^{t}Bu	Me	Mesityl	25.5	3.6	

We next considered catalysts **C13**-**C26** obtained through variations of the phosphine phenyl groups in the **C1** catalyst (Figure S11 and Table S4; Supporting Information). Predicted reactivities and selectivities for these catalysts were in general unremarkable relative to **C1** with the exception of **C25**. Catalyst **C25** ($\Delta G^{\ddagger}$ = 25.4 kcal/mol and $\Delta\Delta G$ = 2.6 kcal/mol; Table 1) which places mesityl groups on the phosphines was predicted to be comparable to **C3** catalyst in terms of reactivity and stereoselectivity. Finally, catalysts **C26**-**C35** were generated by replacing ^{t}Bu with Me at phenolate *para* positions; and including a variety of electron-withdrawing and electron-donating substituents at the *para* and 2,4,6-positions of the phosphine phenyl groups (Figure S11 and Table S4; Supporting Information). Catalyst **C35**, again with phosphine mesityl groups ($\Delta G^{\ddagger}$ = 25.4 kcal/mol and $\Delta\Delta G$ = 3.6 kcal/mol; Table 1), performed equivalently to **C25**, indicating the relative unimportance of the *para*-phenolate substituent with respect to steric bulk.

Conclusion

Density functional characterization of the mechanism of indium(III)phosphasalen catalyzed copolymerization of CO_2/cyclohexene oxide (CHO) distinguishes a mechanism where the turnover-limiting step involves a dissociated carbonate functionality ring-opening CHO coordinated to a mononuclear catalyst. Levels of predicted isotacticity associated with this step are in good agreement with experiment for the known **C1** catalyst and the stereochemical influences of local catalyst configuration and chain-end configuration are found to be roughly equal in magnitude. For known catalysts replacing ^{t}Bu in **C1** with amyl (**C2**) and cumyl (**C3**) groups, trends

in reactivities and isoselectivities were well reproduced. Increased differentiation in distortion energies for the phosphasalen ligand and CHO substrate were identified as contributing to improved reactivity and isoselectivity for **C3**. In addition, replacing phosphine phenyl groups with mesityl groups is predicted to increase stereoselectivity; this prediction remains to be experimentally realized.

Supporting Information. The Supporting Information is available free of charge via the Internet at http://pubs.acs.org

Schemes and energetics of higher energy alternative pathway, energetics details of stationary points and details of conformational analysis (PDF)

Optimized cartesian coordinates (xyz)

Corresponding Author

*Yernaidu Reddi, yreddi@umn.edu

ORCID

Yernaidu Reddi: 0000-0002-6743-9582

Christopher J. Cramer: 0000-0001-5048-1859

Acknowledgements

We acknowledge our funding source, the National Science Foundation Center for Sustainable Polymers at the University of Minnesota, which is a National Science Foundation supported Center for Chemical Innovation (CHE-1901635). We thank the Minnesota Supercomputing Institute (MSI) for providing key computational resources.

References

(1) (a) Hepburn, C.; Adlen, E.; Beddington, J.; Carter, E. A.; Fuss, S.; Dowell, N. M.; Minx, J. C.; Smith, P.; Williams, C. K. The technological and economic prospects for CO_2 utilization and removal. *Nature* **2019**, *575*, 87–97. (b) Artz, J.; Müller, T. E.; Thenert, K.; Kleinekorte, J.; Meys, R.; Sternberg, A.; Bardow, A.; Leitner, W. Sustainable Conversion of Carbon Dioxide: An Integrated Review of Catalysis and Life Cycle Assessment. *Chem. Rev.* **2018**, *118*, 434– 504. (c) Grignard, B.; Gennen, S.; Jerome, C.; Kleij, A. W.; Detrembleur, C. Advances in the use of CO_2 as a renewable feedstock for the synthesis of polymers. *Chem. Soc. Rev.* **2019**, *48*, 4466– 4514. (d) Plaza, M. G.; Martínez, S.; Rubiera, F. CO_2 Capture, Use, and Storage in the Cement Industry: State of the Art and Expectations. *Energies* **2020**, *13*, 5692. (e) Cao, H.; Wang, X. Carbon dioxide copolymers: Emerging sustainable materials for versatile applications. *SusMat*. **2021**, *1*, 88-104. (f) Gao, W.; Liang, S.; Wang, R.; Jiang, Q.; Zhang, Y.; Zheng, Q.; Xie, B.; Toe, C. Y.; Zhu, X.; Wang, J.; Huang, L.; Gao, Y.; Wang, Z.; Jo, C.; Wang, Q.; Wang, L.; Liu, Y.; Louis, B.; Scott, J.; Roger, A. C.; Amal, R.; He, H.; Park, S. E. Industrial carbon dioxide capture and utilization: state of the art and future challenges. *Chem. Soc. Rev*., **2020**, *49*, 8584-8686. (g) Coates, G. W.; Getzler, Y. D. Y.L. Chemical recycling to monomer for an ideal, circular polymer economy. *Nat. Rev. Mater.* **2020**, *5*, 501-516.

(2) (a) Inoue, S.; Koinuma, H.; Tsuruta, T. Copolymerization of carbon dioxide and epoxide. *J. Polym. Sci., Part B: Polym. Lett*. **1969**, *7*, 287. (b) Inoue, S.; Koinuma, H.; Tsuruta, T. Copolymerization of carbon dioxide and epoxide with organometallic compounds. *Makromol. Chem*. **1969**, *130*, 210.

(3) (a) Sulley, G. S.; Gregory, G. L.; Chen, T. T. D.; Peña Carrodeguas, L.; Trott, G.; Santmarti, A.; Lee, K.-Y.; Terrill, N. J.; Williams, C. K. Switchable Catalysis Improves the Properties of CO_2-Derived Polymers: Poly(cyclohexene carbonate-b-ε-decalactone-b-cyclohexene carbonate)

Adhesives, Elastomers, and Toughened Plastics. *J. Am. Chem. Soc*. **2020**, *142*, 4367– 4378. (b) Stosser, T.; Li, C.; Unruangsri, J.; Saini, P. K.; Sablong, R. J.; Meier, M. A. R.; Williams, C. K.; Koning, C. Bio-derived polymers for coating applications: comparing poly(limonene carbonate) and poly(cyclohexadiene carbonate). *Polym. Chem.* **2017**, *8*, 6099–6105. (c) Luinstra, G. A. Poly(propylene carbonate), old copolymers of propylene oxide and carbon dioxide with new interests: catalysis and material properties. *Polym. Rev.* **2018**, *48*, 192–219. (d) Scharfenberg, M.; Hilf, J.; Frey, H. Functional polycarbonates from carbon dioxide and tailored epoxide monomers: degradable materials and their application potential. *Adv. Funct. Mater.* **2018**, *28*, 1704302.

(4) (a) Darensbourg, D. J.; Mackiewicz, R. M.; Phelps, A. L.; Billodeaux, D. R. Copolymerization of CO_2 and Epoxides Catalyzed by Metal Salen Complexes. *Acc. Chem. Res*. **2004**, *37*, 836-844. (b) Sugimoto, H.; Inoue, S. Copolymerization of carbon dioxide and epoxide. *J. Polym. Sci., Part A: Polym. Chem*. **2004**, *42*, 5561-5573. (c) Coates, G. W.; Moore, D. R. Discrete metal-based catalysts for the copolymerization of CO_2 and epoxides: discovery, reactivity, optimization, and mechanism. *Angew. Chem., Int. Ed.* **2004**, *43*, 6618-6639. (d) Darensbourg, D. J. Making Plastics from Carbon Dioxide: Salen Metal Complexes as Catalysts for the Production of Polycarbonates from Epoxides and CO_2. *Chem. Rev*. **2007**, *107*, 2388-2410. (e) Kember, M. R.; Buchard, A.; Williams, C. K. Catalysts for CO2/epoxide copolymerisation. *Chem. Commun*. **2011**, *47*, 141-163. (f) Lu, X. B.; Ren, W. M.; Wu, G. P. CO_2 Copolymers from Epoxides: Catalyst Activity, Product Selectivity, and Stereochemistry Control. *Acc. Chem. Res*. **2012**, *45*, 1721-1735. (g) Lu, X. B.; Darensbourg, D. J. Cobalt catalysts for the coupling of CO2 and epoxides to provide polycarbonates and cyclic carbonates. *Chem. Soc. Rev*. **2012**, *41*, 1462-1484. (h) Kielland, N.; Whiteoak, C. J.; Kleij, A. W. Stereoselective Synthesis with Carbon Dioxide. *Adv. Synth. Catal*. **2013**, *355*, 2115-2138. (i) Raman, S. K.; Deacy, A. C.; Carrodeguas, L. P.; Reis, N. V.; Kerr, R.

W. F.; Phanopoulos, A.; Morton, S.; Davidson, M. G.; Williams, C. K. Ti(IV)–Tris(phenolate) Catalyst Systems for the Ring-Opening Copolymerization of Cyclohexene Oxide and Carbon Dioxide. *Organometallics* **2020**, *39*, 1619–1627. (j) Paul, S.; Zhu, Y. Q.; Romain, C.; Brooks, R.; Saini, P. K.; Williams, C. K. Ring-opening copolymerization (ROCOP): synthesis and properties of polyesters and polycarbonates. *Chem. Commun*. **2015**, *51*, 6459–6479. (k) Kamphuis, A. J.; Picchioni, F.; Pescarmona, P. P. CO_2-fixation into cyclic and polymeric carbonates: principles and applications. *Green Chem.* **2019**, *21*, 406– 448. (j) Martin, C.; Fiorani, G.; Kleij, A. W. Recent Advances in the Catalytic Preparation of Cyclic Organic Carbonates. *ACS Catal.* **2015**, *5*, 1353– 1370. (k) Deacy A. C.; Moreby, E.; Phanopoulos, A.; Williams C. K. Co(III)/Alkali-Metal(I) heterodinuclear catalysts for the ring-opening copolymerization of CO_2 and propylene oxide. *J. Am. Chem. Soc*., **2020**, *142*, 19150-19160. (l) Liu, F.; Gu, Y.; Zhao, P.; Gao, J.; Liu, M. Cooperative Conversion of CO_2 to Cyclic Carbonates in Dual-Ionic Ammonium Salts Catalytic Medium at Ambient Temperature. *ACS Sustainable Chem. Eng.* **2019,** *7*, 5940-5945.

(5) Luinstra, G. Poly(Propylene Carbonate), Old Copolymers of Propylene Oxide and Carbon Dioxide with New Interests: Catalysis and Material Properties. *Polym. Rev*. **2008**, *48*, 192-219.

(6) (a) Gomez, F. J.; Waymouth, R. M. Catalysts Rise to the Challenge. *Science* **2002**, *295*, 635-636. (b) Nakano, K.; Kosaka, N.; Hiyama, T.; Nozaki, K. Metal-catalyzed synthesis of stereoregular polyketones, polyesters, and polycarbonates. *Dalton Trans*. **2003**, 4039-4050.

(7) (a) Cheng, M.; Darling, N. A.; Lobkovsky, E. B.; Coates, G. W. Enantiomerically-enriched organic reagents *via* polymer synthesis: enantioselective copolymerization of cycloalkene oxides and CO_2 using homogeneous, zinc-based catalysts. *Chem. Commun*. **2000**, 2007-2008. (b) Darensbourg, D. J.; Chung, W.-C.; Yeung, A. D.; Luna, M. Dramatic Behavioral Differences of

the Copolymerization Reactions of 1,4-Cyclohexadiene and 1,3-Cyclohexadiene Oxides with Carbon Dioxide. *Macromolecules* **2015,** *48*, 1679-1687. (c) Asaba, H.; Iwasaki, T.; Hatazawa, M.; Deng, J.; Nagae, H.; Mashima, K.; Nozaki, K. Alternating Copolymerization of CO_2 and Cyclohexene Oxide Catalyzed by Cobalt-Lanthanide Mixed Multinuclear Complexes *Inorg. Chem*. **2020**, *59*, 7928–7933. (d) Deng, J.; Ratanasak, M.; Sako, Y.; Tokuda, H.; Maeda, C.; Hasegawa, J.; Nozaki, K.; Ema T. Aluminum Porphyrins with Quaternary Ammonium Halides as Catalysts for Copolymerization of Cyclohexene Oxide and CO_2: Metal–Ligand Cooperative Catalysis. *Chem. Sci.* **2020**, *11*, 5669–5675. (e) Auriemma, F.; De Rosa, C.: Di Caprio, M. R.; Di Girolamo, R.; Ellis, W. C.; Coates, G. W. Stereocomplexed Poly(Limonene Carbonate): A Unique Example of the Cocrystallization of Amorphous Enantiomeric Polymers *Angew. Chem. Int. Ed.*, **2015**, *54*, 1215–1218. (f) Ellis, W. C.; Jung, Y.; Mulzer, M.; Di Girolamo, R.; Lobkovsky, E. B.; Coates, G. W. Copolymerization of CO_2 and *meso* epoxides using enantioselective β-diiminate catalysts: a route to highly isotactic polycarbonates. *Chem. Sci.*, **2014**, *5*, 4004-4011. (g) Carrodeguas, L. P.; Chen, T. T. D.; Gregory, G. L.; Sulley, G. S.; Williams, C. K. High elasticity, chemically recyclable, thermoplastics from bio-based monomers: carbon dioxide, limonene oxide and epsilon-decalactone, *Green Chem.*, **2020**, *22*, 8298-8307. (h) Deacy, A. C.; Kilpatrick, A. F. R.; Regoutz, A.; Williams, C. K. Understanding metal synergy in heterodinuclear catalysts for the copolymerization of CO_2 and epoxides, *Nat. Chem*., **2020**, *12*, 372-380. (i) Darensbourg, D. J. Making plastics from carbon dioxide: salen metal complexes as catalysts for the production of polycarbonates from epoxides and CO_2. *Chem. Rev.* **2007**, *107*, 2388-2410. (j) Romain, C.; Garden, J.A.; Trott, G.; Buchard, A.; White, A. J. P.; Williams, C. K. Di-Zinc-Aryl Complexes: CO_2 Insertions and Applications in Polymerisation Catalysis, *Chem. Eur. J*., **2017**, *23*, 7367-7376. (k) Cao, H.; Qin, Y.; Zhuo, C.; Wang, X.; Wang, F. Homogeneous Metallic Oligomer Catalyst

with Multisite Intramolecular Cooperativity for the Synthesis of CO_2-Based Polymers. *ACS Catal*., **2019**, *9*, 8669-8676. (l) Dean, R. K.; Dawe, L. N.; Kozak, C. M. Copolymerization of Cyclohexene Oxide and CO_2 with a Chromium Diamine-bis(phenolate) Catalyst. *Inorg. Chem.* **2012,** *51*, 9095-9103. (m) Shi, Z.; Jiang, Q.; Song, Z.; Wang, Z.; Gao, C. Dinuclear iron(iii) complexes bearing phenylene-bridged bis(amino triphenolate) ligands as catalysts for the copolymerization of cyclohexene oxide with carbon dioxide or phthalic anhydride , *Polym. Chem*., **2018**, *9*, 4733-4743. (n) Monica, F. D.; Maity, B.; Pehl, T.; Buonerba, A.; De Nisi, A.; Monari, M.; Grassi, A.; Rieger, B.; Cavallo, L.; Capacchione, C. [OSSO]-Type Iron(III) Complexes for the Low-Pressure Reaction of Carbon Dioxide with Epoxides: Catalytic Activity, Reaction Kinetics, and Computational Study, *ACS Catal*., **2018**, *8*, 6882-6893.

(8) (a) Myers, D.; White, A. J. P.; Forsyth, C. M.; Bown, M.; Williams, C. K. Phosphasalen Indium Complexes Showing High Rates and Isoselectivities in rac-Lactide Polymerizations, *Angew. Chem. Int. Ed*., **2017**, *56*, 5277-5282. (b) Douglas, A. F.; Patrick, B. O.; Mehrkhodavandi, P. A Highly Active Chiral Indium Catalyst for Living Lactide Polymerization. *Angew. Chem. Int. Ed.* **2008**, *47*, 2290–2293. (c) Bakewell, C.; White, A. J. P.; Long, N. J.; Williams, C. K. Scandium and Yttrium Phosphasalen Complexes as Initiators for Ring-Opening Polymerization of Cyclic Esters. *Inorg. Chem.* **2015**, *54*, 2204–2212. (d) Bakewell, C.; White, A. J. P.; Long, N. J.; Williams, C. K. Metal-Size Influence in Iso-Selective Lactide Polymerization. *Angew. Chem. Int. Ed.* **2014**, *53*, 9226–9230. (e) Yuntawattana, N.; McGuire, T. M.; Durr, C. B.; Buchard, A.; Williams, C. K. Indium phosphasalen catalysts showing high isoselectivity and activity in racemic lactide and lactone ring opening polymerizations, *Catal. Sci. Technol.*, **2020**, *10*, 7226-7239.

(9) Thevenon, A.; Cyriac, A.; Myers, D.; White, A. J. P.; Durr, C. B.; Williams, C. K. Indium Catalysts for Low-Pressure CO_2/Epoxide Ring-Opening Copolymerization: Evidence for a Mononuclear Mechanism? *J. Am. Chem. Soc*., **2018**, *140*, 6893-6903.

(10) (a) Shao, H.; Reddi, Y.; Cramer, C. J. Modeling the Mechanism of CO_2/Cyclohexene Oxide Copolymerization Catalyzed by Chiral Zinc β-Diiminates: Factors Affecting Reactivity and Isotacticity. *ACS Catal.* **2020**, *10*, 8870-8879. (b) González-Fabra, J.; Castro-Gómez, F.; Kleij, A. W.; Bo, C. Mechanistic Insights into the Carbon Dioxide/Cyclohexene Oxide Copolymerization Reaction: Is One Metal Center Enough? *Chem. Sus. Chem.* **2017**, *10*, 1233-1240. (c) Peña Carrodeguas, L.; González-Fabra, J.; Castro-Gómez, F.; Bo, C.; Kleij, A. W. Al^{III}-Catalysed Formation of Poly(limonene)carbonate: DFT Analysis of the Origin of Stereoregularity. *Chem. Eur. J.* **2015**, ***21***, 6115-5122.

(11) Zhao, Y.; Truhlar, D. G. The M06 suite of density functionals for main group thermochemistry, thermochemical kinetics, noncovalent interactions, excited states, and transition elements: Two new functionals and systematic testing of four M06-class functionals and 12 other functionals. *Theor. Chem Acc.* **2006**, *120*, 215–241.

(12) Grimme, S.; Antony, J.; Ehrlich, S.; Krieg, H. A consistent and accurate ab initio parametrization of density functional dispersion correction (DFT-D) for the 94 elements H-Pu. *J. Chem. Phys.* **2010**, *132*, 154104.

(13) Weigend, F.; Ahlrichs, R. Balanced basis sets of split valence, triple zeta valence and quadruple zeta valence quality for H to Rn: Design and assessment of accuracy. *Phys. Chem. Chem. Phys.* **2005**, *7*, 3297– 3305.

(14) Marenich, A. V.; Cramer, C. J.; Truhlar, D. G. Universal Solvation Model Based on Solute Electron Density and on a Continuum Model of the Solvent Defined by the Bulk Dielectric Constant and Atomic Surface Tensions. *J. Phys. Chem. B* **2009**, *113*, 6378– 6396.

(15) Frisch, M. J.; Trucks, G. W.; Schlegel, H. B.; Scuseria, G. E.; Robb, M. A.; Cheeseman, J. R.; Scalmani, G.; Barone, V.; Petersson, G. A.; Nakatsuji, H.; Li, X.; Caricato, M.; Marenich, A. V.; Bloino, J.; Janesko, B. G.; Gomperts, R.; Mennucci, B.; Hratchian, H. P.; Ortiz, J. V.; Izmaylov, A. F.; Sonnenberg, J. L.; Williams-Young, D.; Ding, F.; Lipparini, F.; Egidi, F.; Goings, J.; Peng, B.; Petrone, A.; Henderson, T.; Ranasinghe, D.; Zakrzewski, V. G; Gao, J.; Rega, N.; Zheng, G.; Liang, W.; Hada, M.; Ehara, M.; Toyota, K.; Fukuda, R.; Hasegawa, J.; Ishida, M.; Nakajima, T.; Honda, Y.; Kitao, O.; Nakai, H.; Vreven, T.; Throssell, K.; Montgomery, J. A., Jr.; Peralta, J. E.; Ogliaro, F.; Bearpark, M. J.; Heyd, J. J.; Brothers, E. N.; Kudin, K. N.; Staroverov, V. N.; Keith, T. A.; Kobayashi, R.; Normand, J.; Raghavachari, K.; Rendell, A. P.; Burant, J. C.; Iyengar, S. S.; Tomasi, J.; Cossi, M.; Millam, J. M.; Klene, M.; Adamo, C.; Cammi, R.; Ochterski, J. W.; Martin, R. L.; Morokuma, K.; Farkas, O.; Foresman, J. B.; Fox, D. J. Gaussian 16, Revision C.01, Gaussian, Inc., Wallingford CT, 2016.

(16) Chai, J. D.; Head-Gordon, M. Long-range corrected hybrid density functionals with damped atom–atom dispersion corrections. *Phys. Chem. Chem. Phys.* **2008**, *10*, 6615– 6620.

(17) Adamo, C.; Barone, V. Toward reliable density functional methods without adjustable parameters: The PBE0 model. *J. Chem. Phys.* **1999**, *110*, 6158– 6170.

(18) Yu, H. S.; He, X.; Li, S. L.; Truhlar, D. G. MN15: A Kohn-Sham Global-Hybrid ExchangeCorrelation Density Functional with Broad Accuracy for Multi-Reference and Single-Reference Systems and Noncovalent Interactions. *Chem. Sci*. **2016**, *7*, 5032–5051.

(19) Marenich, A. V.; Jerome, S. V.; Cramer, C. J.; Truhlar, D. G. Charge model 5: An extension of Hirshfeld population analysis for the accurate description of molecular interactions in gaseous and condensed phases. *J. Chem. Theory Comput.* **2012**, *8*, 527– 541.

(20) (a) Martinez, H.; Miró, P.; Charbonneau, P.; Hillmyer, M. A.; Cramer, C. J. Selectivity in Ring-opening Metathesis Polymerization of Z-Cyclooctenes Catalyzed by a Second-generation Grubbs Catalyst *ACS Catal*. **2012**, *2*, 2547– 2556. (b) Martinez, H.; Hillmyer, M. A.; Cramer, C. J. Factors Controlling the Regio- and Stereoselectivity of the Ring-Opening Metathesis Polymerization of 3-Substituted Cyclooctenes by Monoaryloxide Pyrrolide Imido Alkylidene (MAP) Tungsten Catalysts *J. Org. Chem*. **2014**, *79*, 11940–11948.

(21) Contreras-Garcia, J.; Johnson, E. R.; Keinan, S.; Chaudret, R.; Piquemal, J.-P.; Beratan, D. N.; Yang, W. NCIPLOT: A Program for Plotting Noncovalent Interaction Regions. *J. Chem. Theory Comput*. **2011**, *7*, 625−632.

(22) (a) Jiang, L.; Althoff, E. A.; Clemente, F. R.; Doyle, L.; Rothlisberger, D.; Zanghellini, A.; Gallaher, J. L.; Betker, J. L.; Tanaka, F.; Barbas, III, C. F.; Hilvert, D.; Houk, K. N.; Stoddard, B. L.; Baker, D. De Novo Computational Design of Retro-Aldol Enzymes *Science*, **2008**, *319*, 1387-1391. (b) Meng, S.-S.; Yu, P.; Yu, Y.-Z.; Liang, Y.; Houk, K. N.; Zheng, W.-H. Computational Design of Enhanced Enantioselectivity in Chiral Phosphoric Acid-Catalyzed Oxidative Desymmetrization of 1,3-Diol Acetals *J. Am. Chem. Soc.* **2020**, *142*, 8506-8513. (c) Reddi, Y.; Tsai, C. C.; Avila, C. M.; Toste, F. D.; Sunoj, R. B. Harnessing Noncovalent Interactions in Dual-Catalytic Enantioselective Heck–Matsuda Arylation. *J. Am. Chem. Soc.* **2019**, *141*, 998– 1009. (d) Rooks, B. J.; Haas, M. R.; Sepúlveda, D.; Lu, T.; Wheeler, S. E. Prospects for the Computational Design of Bipyridine N,N′-Dioxide Catalysts for Asymmetric Propargylation Reactions *ACS Catalysis* **2015**, *5*, 272-280.

TOC

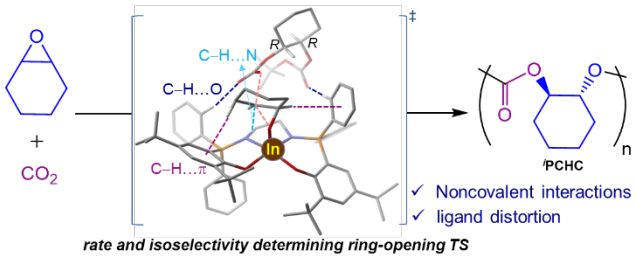
C–H…N
C–H…O
C–H…π
In
R
R
‡
+
CO2
n
iPCHC
✓ Noncovalent interactions
✓ ligand distortion
rate and isoselectivity determining ring-opening TS